

Reinforcement Learning from Multiple Sensors via Joint Representations

Philipp Becker¹ Sebastian Markgraf¹ Fabian Otto^{2,3} Gerhard Neumann¹

Abstract

In many scenarios, observations from more than one sensor modality are available for reinforcement learning (RL). For example, many agents can perceive their internal state via proprioceptive sensors but must infer the environment’s state from high-dimensional observations such as images. For image-based RL, a variety of self-supervised representation learning approaches exist to improve performance and sample complexity. These approaches learn the image representation in isolation. However, including proprioception can help representation learning algorithms to focus on relevant aspects and guide them toward finding better representations. Hence, in this work, we propose using *Recurrent State Space Models* to fuse all available sensory information into a single consistent representation. We combine reconstruction-based and contrastive approaches for training, which allows using the most appropriate method for each sensor modality. For example, we can use reconstruction for proprioception and a contrastive loss for images. We demonstrate the benefits of utilizing proprioception in learning representations for RL on a large set of experiments. Furthermore, we show that our joint representations significantly improve performance compared to a post hoc combination of image representations and proprioception.

1. Introduction

Learning concise representations of high-dimensional images has led to considerable advances in reinforcement learning (RL) from pixels. However, while images are crucial to perceive an agent’s surroundings in unstructured environments, they are often not the only available source of information. Most realistic agents can additionally observe

¹Karlsruhe Institute of Technology, Germany ²Bosch Center for Artificial Intelligence, Germany ³University of Tübingen, Germany. Correspondence to: Philipp Becker <philipp.becker@kit.edu>.

their internal state directly using the sensing in their actuators, inertial measurement units, force and torque sensors, or other forms of proprioceptive sensing. So far, most RL approaches that use representations learn them for a single high-dimensional sensor, such as a camera, in isolation (Hafner et al., 2019; Srinivas et al., 2020; Zhang et al., 2020). In this work, we study how to best combine these different sensors into a representation that facilitates successful and data-efficient RL.

We propose using State Space Models to learn a single representation of all available sensors. The state space formulation lends itself naturally to the problem at hand - accumulating information across multiple sensors and time to form a single concise representation of the entire system state. By building on *Recurrent State Space Models (RSSMs)* (Hafner et al., 2019), this approach provides a scalable basis for RL in tasks with complex observations and dynamics.

Given this formalism, the question of training the representation arises. Previous works suggest using either reconstruction (Hafner et al., 2019; 2021) or contrastive methods (Hafner et al., 2020; Ma et al., 2020; Nguyen et al., 2021) to train RSSMs, both of which have their strengths and weaknesses. Reconstruction is a powerful tool if observations contain only task-relevant or static elements. Yet, it can fail to learn good representations if observations are noisy or include distracting elements (Zhang et al., 2020; Ma et al., 2020; Deng et al., 2022). In such cases, contrastive methods can ignore irrelevant parts of the observation and still learn useful representations. Furthermore, reconstruction creates an overhead when learning a representation, but the resulting learning approach is relatively stable. On the other hand, contrastive methods require less overhead but more care during training to prevent the representation from collapsing. Which loss is preferable thus depends on the kind of observations at hand. Consequently, we propose to choose the loss for each sensor individually, according to the specific characteristics of the observation. The common approach to train RSSMs is variational inference, which maximizes a lower bound to the data log-likelihood. Using this bound involves computing the likelihood of the individual observations under the model, which requires explicit reconstruction. However, we can replace these likelihood terms with mutual information terms, resulting in a contrastive loss (Hafner et al., 2020; Ma et al., 2020).

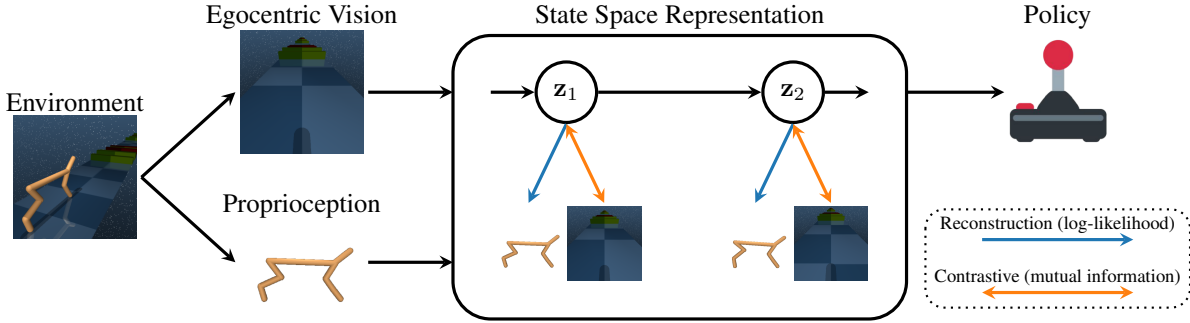


Figure 1. For many reinforcement learning problems, more than one sensor modality is available. For example, in the shown locomotion task, the robot has an egocentric vision to perceive its environment but directly observes its proprioceptive state, i.e., the position and velocity of its body parts. We propose learning a joint representation of all available sensor sources as the basis for decision-making by a policy. We build on *Recurrent State Space Models* to accumulate information across sensors and time and use a combination of contrastive and reconstruction-based losses for training. Our experiments show that such jointly learned representations can significantly improve the performance of downstream policies.

Contrastive predictive coding (Oord et al., 2018) offers an alternative to the variational approach of training *RSSMs* (Nguyen et al., 2021; Srivastava et al., 2021). Those methods train the *RSSMs*’ system dynamics by explicitly predicting the future latent state and maximizing the agreement of the prediction with future observations. As recent literature is inconclusive about whether the variational or the predictive approach is preferable, we evaluate our representation learning using both methods. To act based on our representations, we train a policy using the model-free Soft Actor-Critic (SAC) approach, as purely model-based *latent imagination* (Hafner et al., 2020) tends to underperform with contrastively learned *RSSMs* (Hafner et al., 2020; Ma et al., 2020). Figure 1 shows an overview of our approach.

We evaluate our approach on several tasks from the DeepMind Control (DMC) Suite (Tassa et al., 2018) and compare it to several baselines for image-based RL. To test the ability of all approaches to cope with distractions and missing information, we modify the DMC Suite tasks to use natural video backgrounds and occlusions. While previous contrastive approaches tackled the natural video background case (Zhang et al., 2020; Ma et al., 2020; Nguyen et al., 2021; Deng et al., 2022), we are the first to consider occlusions. Those significantly increase the difficulty of the tasks. As of now, they are only solvable by using the additional proprioception to guide representation learning. Furthermore, we evaluate our method using a new Locomotion Suite and a challenging robot manipulation task. For the Locomotion Suite, agents must combine proprioception and egocentric vision to move and navigate. Our experiments are inconclusive about whether to use variational or predictive methods. However, they show learning joint representations of all sensors is beneficial in either case. Doing so outperforms both exclusively using images and concatenating proprioception with independently learned image representations.

While results increase particularly in settings where a combination of images and proprioception is necessary for decision-making, we also observe significant performance improvements when all information is available through images. These findings show that including proprioception can indeed guide representation learning algorithms to find better representations for RL.

We summarize our contributions as follows:

- We propose using *RSSMs* to learn joint representations of multiple observations emitted by different sensors over time.
- We introduce a general framework for training such joint representations by combining reconstruction-based and contrastive approaches.
- We show that such joint representations outperform concatenating proprioception and independent image representations. In addition, using proprioception in representation learning enables solving tasks that are currently not solvable with only image representations.

2. Related Work

Representations for Reinforcement Learning. Many recent approaches use ideas from generative (Wahlström et al., 2015; Watter et al., 2015; Banijamali et al., 2018; Lee et al., 2020; Yarats et al., 2021b) and self-supervised representation learning (Zhang et al., 2020; Srinivas et al., 2020; Yarats et al., 2021a; You et al., 2022) to improve performance, sample efficiency, and generalization of RL from images. Particularly relevant for this work are those based on *Recurrent State Space Models* (*RSSMs*). When proposing the *RSSM*, Hafner et al. (2019) used a generative approach. They formulated their objective as auto-encoding variational

inference, which trains the representation by reconstructing observations. Such reconstruction-based approaches have limitations with observations containing noise or many task-irrelevant details. As a remedy, Hafner et al. (2020) proposed a contrastive alternative based on mutual information and the InfoNCE estimator (Poole et al., 2019). Ma et al. (2020) refined this approach and improved results by modifying the policy learning mechanism. Using a different motivation, namely contrastive predictive coding (Oord et al., 2018), Okada & Taniguchi (2021); Nguyen et al. (2021); Srivastava et al. (2021) proposed alternative contrastive learning objectives for *RSSMs*. In this work, we leverage the variational and predictive coding paradigms and show that joint representations improve performance for both. Other recent approaches for learning *RSSMs*, e. g., using prototypical representations (Deng et al., 2022) or explicit factorizations to remove task-irrelevant aspects (Wang et al., 2022), are orthogonal to our work and may be combined with it in the future.

Out of these works, only Srivastava et al. (2021) consider using additional proprioceptive information. Yet, they did so only in a single experiment, without deeper analysis or elaboration on the topic. Further, they did not compare to the concatenation of image representations and proprioception.

Sensor Fusion in Reinforcement Learning. Many application-driven approaches to visual RL for robots use proprioception to solve their specific tasks (Finn et al., 2016; Levine et al., 2016; Kalashnikov et al., 2018; Xiao et al., 2022; Fu et al., 2022). Yet, they usually do not use dedicated representation learning or concatenate image representations and proprioception. There are notable exceptions (Wu et al., 2022; Becker & Neumann, 2022), which use *RSSMs* with images and proprioception and thus learn joint representations. However, both put little emphasis on the fusion itself, only use reconstruction-based losses, and focus on learning with real-world robots (Wu et al., 2022) or analyze the *RSSM*'s assumptions (Becker & Neumann, 2022). We instead focus on learning joint representations and study different ways of training them. Our results show that such representations can significantly outperform concatenating image representations and proprioception.

Multimodal Representation Learning. Representation learning from multiple modalities has widespread applications in general machine learning, where methods such as *CLIP* (Radford et al., 2021) combine language concepts with the semantic knowledge of images and allow language-based image generation (Ramesh et al., 2022). For robotics, Brohan et al. (2022); Mees et al. (2022) combined language models with the robot's perception for natural language-guided manipulation tasks using imitation learning. In contrast, we work in an online RL setting and mainly consider different modalities, namely images, and proprioception.

3. Learning Representation from Multiple Sensors with State Space Models

Given trajectories of observations $\mathbf{o}_{1:T} = \{\mathbf{o}_t\}_{t=1:T}$ and actions $\mathbf{a}_{1:T} = \{\mathbf{a}_t\}_{t=1:T}$ we aim to learn a state representation that is well suited for RL. We assume the observations stem from K different sensor sources, $\mathbf{o}_t = \{\mathbf{o}_t^{(k)}\}_{k=1:K}$, where the individual $\mathbf{o}_t^{(k)}$ might be high dimensional, noisy, and contain only partial information about the system. Further, even the whole observation \mathbf{o}_t may not contain all the information necessary for acting optimally, i. e., the environment is partially observable, and the representation needs to accumulate information over time.

Our goal is to learn a concise, low dimensional representation $\phi(\mathbf{o}_{1:t}, \mathbf{a}_{1:t-1})$ that accumulates all relevant information until time step t . We provide this representation to a policy $\pi(\mathbf{a}_t | \phi(\mathbf{o}_{1:t}, \mathbf{a}_{1:t-1}))$ which aims at maximizing the expected return in a given RL problem. Here, we have a cyclic dependency, as the policy collects the trajectories to learn the representation by acting in the environment. In this setting, the policy's return and the sample complexity of the entire system determine what constitutes a *good* representation.

3.1. Representations from State Space Models

State Space Models (SSMs) (Murphy, 2012) are commonly used to model time series data and naturally lend themselves to sensor fusion and information accumulation problems. We assume a latent state variable, \mathbf{z}_t , which evolves according to some Markovian dynamics $p(\mathbf{z}_{t+1} | \mathbf{z}_t, \mathbf{a}_t)$ given an action \mathbf{a}_t . At each time step t , each of the K observations are generated from the latent state by an observation model $p^{(k)}(\mathbf{o}_t^{(k)} | \mathbf{z}_t)$ and the initial state is distributed according to $p(\mathbf{z}_0)$. Thus, the joint distribution over a sequence of latent states and observations is assumed to factorize as

$$\begin{aligned} & p(\mathbf{z}_{1:T}, \mathbf{o}_{1:T} | \mathbf{a}_{1:T}) \\ &= p(\mathbf{z}_0) \prod_{t=1}^T p(\mathbf{z}_t | \mathbf{a}_{t-1}, \mathbf{z}_{t-1}) \prod_{t=0}^T \prod_{k=1}^K p_k(\mathbf{o}_t^{(k)} | \mathbf{z}_t). \end{aligned}$$

In this approach, the representation is given by (the parameters of) the belief over the latent state, taking into account all previous actions as well as previous and current observations

$$\phi(\mathbf{o}_{1:t}, \mathbf{a}_{1:t-1}) \hat{=} p(\mathbf{z}_t | \mathbf{a}_{1:t-1}, \mathbf{o}_{1:t}).$$

Yet, due to the nonlinearity of the dynamics and observation models, computing $p(\mathbf{z}_t | \mathbf{a}_{1:t-1}, \mathbf{o}_{1:t})$ is intractable for models of relevant complexity. Thus, we approximate it using a variational distribution $q(\mathbf{z}_t | \mathbf{a}_{1:t-1}, \mathbf{o}_{1:t})$. This variational approximation plays an integral part in training the SSM and is thus readily available to use as input for the policy.

3.2. Instantiating the State Space Model

We build our model on *Recurrent State Space Models (RSSMs)* (Hafner et al., 2019), which serve as the basis for many recent approaches to RL from images. The *RSSM* splits the latent state \mathbf{z}_t into a stochastic part \mathbf{s}_t and a deterministic part \mathbf{h}_t , i.e., $\mathbf{z}_t = \{\mathbf{s}_t, \mathbf{h}_t\}$. Following Hafner et al. (2019; 2020), we assume \mathbf{s}_t to be Gaussian distributed, as the more recently introduced parametrization as a categorical distribution (Hafner et al., 2021) has not been proven beneficial for the continuous control tasks considered in this work. The deterministic part evolves according to $\mathbf{h}_t = g(\mathbf{h}_{t-1}, \mathbf{s}_{t-1}, \mathbf{a}_{t-1})$, where g is implemented as a Gated Recurrent Unit (GRU) (Cho et al., 2014). The stochastic part \mathbf{s}_t only depends on the deterministic part \mathbf{h}_t and is given by a model $p(\mathbf{s}_t|\mathbf{h}_t)$. While the original *RSSM* only has a single observation model $p(\mathbf{o}_t|\mathbf{z}_t)$, we extend it to K models, one for each observation modality $\mathbf{o}_t^{(k)}$.

The variational distribution takes the deterministic part of the state together with the K observations $\mathbf{o}_t = \{\mathbf{o}_t^{(k)}\}_{k=1:K}$ and factorizes as

$$q(\mathbf{z}_{1:t}|\mathbf{o}_{1:t}, \mathbf{a}_{1:t-1}) = \prod_{t=1}^T q(\mathbf{z}_t|\mathbf{z}_{t-1}, \mathbf{a}_{t-1}, \mathbf{o}_t).$$

Compared to the original *RSSM*, we again have to account for multiple observations instead of one. Thus, we first encode each observation individually using a set of K encoders, concatenate their outputs and provide the result to the *RSSM*.

Finally, we also learn a reward model $p(r_t|\mathbf{z}_t)$ to predict the achieved reward from the representation. While this is not necessary for policy learning in our case, it has proven beneficial for representation learning in prior work (Srivastava et al., 2021) and our preliminary experiments.

3.3. Learning the State Space Representation

We combine reconstruction-based and contrastive approaches to train our representations. The contrastive approaches can be based on either a contrastive variational viewpoint (Hafner et al., 2020; Ma et al., 2020) or a contrastive predictive coding (CPC) (Oord et al., 2018) viewpoint (Nguyen et al., 2021; Srivastava et al., 2021). As neither approach decisively outperforms the other, we investigate both methods.

Reconstruction. Originally, Hafner et al. (2019) proposed leveraging a fully generative approach for *RSSMs*. Building on the stochastic variational autoencoding Bayes framework (Kingma & Welling, 2013; Sohn et al., 2015), they derived a variational lower bound. Maximizing this bound simultaneously trains the variational distribution and all parts of the generative model. Given our assumption that the observation factorizes into K independent observations, and after

introducing a likelihood term for the reward model, the loss following from the lower bound is given by

$$\begin{aligned} & \sum_{t=1}^T \left(\left(\sum_{k=1}^K -\mathbb{E} [\log p^{(k)}(\mathbf{o}_t^{(k)}|\mathbf{z}_t)] \right) - \mathbb{E} [\log p(r_t|\mathbf{z}_t)] \right. \\ & \left. + \mathbb{E} [\text{KL} [q(\mathbf{z}_t|\mathbf{z}_{t-1}, \mathbf{a}_{t-1}, \mathbf{o}_t) \parallel p(\mathbf{z}_t|\mathbf{z}_{t-1}, \mathbf{a}_{t-1})]] \right), \quad (1) \end{aligned}$$

where the expectations are formed over the distribution $p(\mathbf{o}_{1:t}, \mathbf{a}_{1:t-1})q(\mathbf{z}_t|\mathbf{o}_{1:t}, \mathbf{a}_{1:t-1})$, i.e., sub-trajectories from a replay buffer and the variational distribution. To optimize this bound, we obtain unbiased gradient estimates using the reparametrization trick (Kingma & Welling, 2013; Rezende et al., 2014), which we then use for stochastic gradient descent.

While this reconstruction-based approach can be highly effective, reconstructing high-dimensional, noisy observations can also cause issues. First, it requires introducing large parameter-rich observation models (usually up-convolutional neural nets for images) solely for representation learning. These observation models are unessential for the downstream usage of the representation and are usually discarded after training. Second, the reconstruction forces the model to capture all details of the observations, which can lead to highly suboptimal representations if images are noisy or contain task-irrelevant distractions.

Contrastive Variational Learning. Contrastive learning can provide a remedy to the previously mentioned problems with reconstruction. The key is that the expected log-likelihood $\mathbb{E} [\log p^{(k)}(\mathbf{o}_t^{(k)}|\mathbf{z}_t)]$ can be replaced with the mutual information (MI) $I(\mathbf{o}_t^{(k)}, \mathbf{z}_t)$ by adding and subtracting the evidence $\log p(\mathbf{o}_t^{(k)})$ (Hafner et al., 2020; Ma et al., 2020)

$$\begin{aligned} & \mathbb{E} \left[\log \frac{p^{(k)}(\mathbf{o}_t^{(k)}|\mathbf{z}_t)}{p(\mathbf{o}_t^{(k)})} + \log p(\mathbf{o}_t^{(k)}) \right] \\ & = \mathbb{E} [I(\mathbf{o}_t^{(k)}, \mathbf{z}_t)] + c. \quad (2) \end{aligned}$$

Intuitively, the MI measures how informative a given latent state is about the corresponding observations. Thus, maximizing it leads to similar latent states for similar sequences of observations and actions.

To estimate the MI we can use the InfoNCE lower bound (Oord et al., 2018; Poole et al., 2019). This approach eliminates the need for reconstruction and instead requires only a score function $f_v^{(k)}(\mathbf{o}_t^{(k)}, \mathbf{z}_t) \mapsto \mathbb{R}_+$. The score function measures the compatibility of pairs of observations and latent states, is trained as described in Section 3.5, and shares large parts of its parameters with the *RSSM*. For further details, we refer to Appendix B.2.

Contrastive Predictive Coding. CPC (Oord et al., 2018) provides an alternative to the contrastive variational approach. The idea is to maximize the MI between the latent variable \mathbf{z}_t and the next observation $\mathbf{o}_{t+1}^{(k)}$, i.e. $I(\mathbf{o}_{t+1}^{(k)}, \mathbf{z}_t)$. While this approach seems similar to contrastive variational learning, there is a crucial conceptual difference. We estimate the MI between the current latent state and the next observation, not the current observation. Thus, we explicitly predict one step ahead to compute the loss. As we use the *RSSM*'s dynamics model for the prediction, this formalism provides a training signal to the dynamics model. However, prior works (Shu et al., 2020; Nguyen et al., 2021; Srivastava et al., 2021) showed that solely optimizing for prediction is insufficient. We follow Srivastava et al. (2021) and regularize the objective further by adding an inverse dynamics predictor $\hat{\mathbf{a}}_t = a(\mathbf{z}_t, \mathbf{z}_{t+1})$, a reward prediction term, and the KL-term from Equation 1 multiplied with a small factor β .

The resulting objective is given by

$$\sum_{t=1}^T \left(\sum_{k=1}^K -\mathbb{E} \left[\hat{I}(\mathbf{o}_{t+1}^{(k)}, \mathbf{z}_t) + \log p(r_t | \mathbf{z}_t) + \|\mathbf{a}_t - \hat{\mathbf{a}}_t\|^2 \right] \right. \\ \left. + \beta \mathbb{E} [\text{KL} [q(\mathbf{z}_t | \mathbf{z}_{t-1}, \mathbf{a}_{t-1}, \mathbf{o}_t) \| p(\mathbf{z}_t | \mathbf{z}_{t-1}, \mathbf{a}_{t-1})]] \right),$$

where $\hat{I}(\mathbf{o}_{t+1}^{(k)}, \mathbf{z}_t)$ is an estimate of $I(\mathbf{o}_{t+1}^{(k)}, \mathbf{z}_t)$. We again use InfoNCE, this time with a score function $f_p^{(k)}(\mathbf{o}_{t+1}^{(k)}, \mathbf{z}_t) \mapsto \mathbb{R}_+$. From an implementation viewpoint, the resulting approach differs only slightly from the variational contrastive one. For CPC approaches, we use a sample from the *RSSM*'s dynamics $p(\mathbf{z}_{t+1} | \mathbf{z}_t, \mathbf{a}_t)$ and for contrastive variational approaches we use a sample from the variational distribution $q(\mathbf{z}_t | \mathbf{z}_{t-1}, \mathbf{a}_{t-1}, \mathbf{o}_t)$.

Reconstruction vs. Contrastive Learning. The question arises in which cases contrastive approaches are better suited than reconstruction-based approaches and vice versa. While contrastive approaches are clearly beneficial for high-dimensional noisy observations, such as images, they might not be the optimal choice for more concise, noise-free observations, e.g., proprioception. We thus propose combining the two approaches and choosing the optimal method for each of the K observations separately.

We already demonstrated how to replace contrastive loss terms based on mutual information with reconstruction terms based on the log-likelihood in Equation 2. Following the same principle, we can turn individual contrastive loss terms into reconstruction terms for the CPC approach. In this case, we use a sample of the dynamics $p(\mathbf{z}_{t+1} | \mathbf{z}_t, \mathbf{a}_t)$ for reconstruction (as opposed to a sample from the variational model for the variational approaches). Using the dynamics here again provides a training signal by explicit one-step-ahead prediction.

3.4. Learning to Act Based on the Representation

We use the parameters of the variational posterior belief $q(\mathbf{z}_t | \mathbf{z}_{t-1}, \mathbf{a}_{t-1}, \mathbf{o}_t)$ as our representation. More specifically, we use the deterministic part of the latent state \mathbf{h}_t as well as the mean of the stochastic part, which we denote as μ_t , i.e. $\phi = \phi(\mathbf{o}_{1:t}, \mathbf{a}_{1:t-1}) = \{\mu_t, \mathbf{h}_t\}$.

Given the representation, we learn a policy $\pi(\mathbf{a} | \phi)$ using Soft Actor-Critic (SAC) (Haarnoja et al., 2018). Here, we use ϕ as input for both the actor and the critic. During training, we alternately update the *RSSM*, actor, and critic for d steps before collecting a new sequence. Here, d is half the length of the previous sequence. The *RSSM* uses only the representation learning loss and gets neither gradients from the actor nor the critic.

3.5. Practical Aspects

Image Augmentation. Following prior works (Srivastava et al., 2021; Deng et al., 2022), we found image augmentation helpful for contrastive approaches. Thus, we use random cropping for the contrastive variational and the CPC approach. During training, crops are randomly selected for each sequence but remain consistent within the sequence. For evaluation, we crop at the center.

InfoNCE and Negative Samples. We estimate the mutual information (MI) using b mini-batches of sub-sequences of length l . After computing the latent estimates, we get $I = b \cdot l$ pairs $(\mathbf{o}_i, \mathbf{z}_i)$, i.e., we use both samples from the elements of the batch as well as all the other time steps within the sequence as negative samples. Using those, the symmetry of MI, the InfoNCE bound (Poole et al., 2019), and either $f = f_v^{(k)}$ or $f = f_p^{(k)}$, we can estimate the MI as

$$0.5 \left(\sum_{i=1}^I \log \frac{f(\mathbf{z}_i, \mathbf{o}_i)}{\sum_{j=1}^I f(\mathbf{z}_j, \mathbf{o}_i)} + \log \frac{f(\mathbf{z}_i, \mathbf{o}_i)}{\sum_{j=1}^I f(\mathbf{z}_i, \mathbf{o}_j)} \right).$$

4. Experiments

We evaluate our joint representation learning approach on several environments from the DeepMind Control (DMC) Suite (Tassa et al., 2018) with different types of image observations, a new Locomotion Suite, and a simulated robot manipulation task. Unless stated otherwise, we train five seeds per task for 10^6 environment steps and evaluate for 20 rollouts every 20,000 step. Following the suggestions from Agarwal et al. (2021), we aggregate the results over all environments in the benchmark suites and report interquartile means and 95% stratified bootstrapped confidence intervals, indicated by shaded areas. Appendix C provides the individual environments results. For hyperparameters, we refer to Appendix B¹. In summary, we compare the following

¹We will provide code with the camera-ready version

approaches:

Joint Representation Learning. We denote all methods that learn joint representations of images and proprioception with $Joint(X)$. Here, X will denote how we trained the representation, which is either reconstruction (R), contrastive variational (CV), contrastive predictive (CPC), or combinations of a contrastive approach and reconstruction, i.e., ($CV+R$) and ($CPC+R$). For these combinations, we use contrastive losses for images and reconstruction for proprioception. Here, the reconstruction uses a sample from the dynamics for ($CPC+R$) while it uses a sample from the variational distribution for ($CV+R$).

Concatenating Representations. One important baseline is concatenating the proprioception to a representation trained solely on images. To ensure a fair comparison, we train this representation using our State-Space approach using only the images. Here, we again use reconstruction and both contrastive methods for training and refer to the resulting approaches as $Concat(R)$, $Concat(CV)$, and $Concat(CPC)$.

Single Observations. We also train policies using only a single sensor to ensure our approaches can exploit the additional information provided by multiple sensors. For the image-only policies, we again use our State-Space representation approach and the different training schemes, resulting in $Img-Only(R)$, $Img-Only(CV)$, and $Img-Only(CPC)$. For the proprioception-only policies (*Proprio-Only*), we use SAC (Haarnoja et al., 2018) directly on the proprioception without learning an explicit representation.

Related Approaches. While we focus on learning joint representations from multiple sensors, we also ensure our method performs comparably or favorably to other recent approaches. We compare against the reconstructing *Dreamer*-v2 (Hafner et al., 2021), the contrastive *DreamerPro* (Deng et al., 2022). Additionally, we compare to *DrQ*-v2 (Yarats et al., 2022), which does not explicitly learn a representation, and extend it to handle both images and proprioception. We introduce a separate encoder for the proprioception and concatenate its output to the output of the original *DrQ*-v2’s image encoder. We refer to the resulting method as (*DrQ*-v2($I+P$)). Additionally, *Img-Only(CPC)* and *Joint(CPC)* closely resemble the approach of (Srivastava et al., 2021). The main differences are that we do not use the critic’s gradients to train the representation and that we adapted the hyperparameters to match those of our other approaches.

4.1. DeepMind Control Suite

For the first experiment, we use seven tasks from the DMC Suite (Tassa et al., 2018). Those are Ball in Cup Catch, Cartpole Swingup, Cheetah Run, Reacher Easy, Walker Walk, Walker Run, and Quadruped Walk. For each task, we split



Figure 2. Examples of the different image types we use with the DMC Suite. **Left:** The standard images as provided by the suite. **Center:** Images with natural video background. We render randomly sampled videos from the Kinetics400 dataset behind the agent to cause visual distractions (Kay et al., 2017). **Right:** Images with occlusions. We render slow-moving disks in front of the agent to occlude relevant parts of the environment.

the state into proprioceptive entries and non-proprioceptive entries. While the former is directly provided, the latter can only be perceived via an additional image. For example, in Cup Catch the cup’s state is proprioceptive while the ball’s state needs to be inferred from the image. Appendix A lists the details for all the above environments. Besides standard images, we run experiments with two types of modified images by adding natural video backgrounds or occlusions. Figure 2 shows examples for Cheetah Run.

Natural Video Background. We render natural videos from the Kinetics400 dataset (Kay et al., 2017) behind the agent. Following, Nguyen et al. (2021); Zhang et al. (2020); Deng et al. (2022) we use the videos from the driving car class and adhere to the train-validation split. Here, the challenge is to learn a representation that allows for efficient policy learning by filtering out as many irrelevant visual details as possible while not ignoring relevant aspects. Methods based on image reconstruction struggle at this task, as the corresponding likelihood maximization treats every pixel as equally important. Thus, it forces the representation to include irrelevant details about the background.

Images with Occlusions. We render occlusions in front of the agent by adding disks that move slowly according to simple linear dynamics. Those occlusions can remove relevant information from the images for multiple consecutive time steps, which decreases observability and increases the task’s complexity. This modification tests the approaches’ capabilities to maintain a consistent representation across multiple time steps and to rely on the dynamics model when certain relevant aspects are missing.

We compare all our methods on all tasks and show an excerpt of the results in Figure 3. Appendix C provides the remaining results. The most important result is that joint representations generally outperform approaches that concatenate image representations and proprioception or use only a single sensor modality. This result holds for all image types independent of using a variational or predictive approach for training. When using only images, our approach

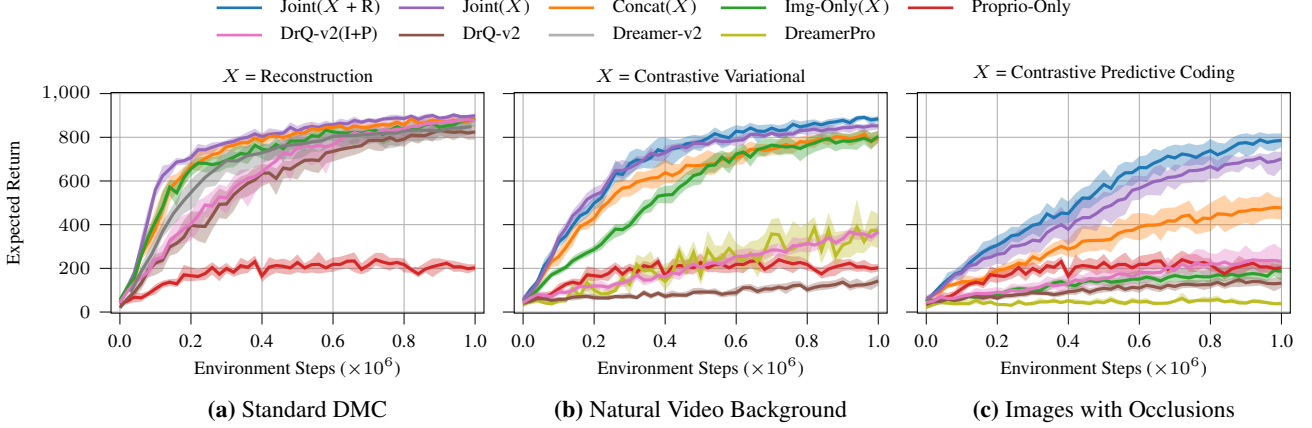


Figure 3. Excerpt of the aggregated results on the standard DMC Suite tasks, with different forms of image observations. In all tasks using proprioception is beneficial. More importantly, learning a joint representation outperforms the concatenation of image representations and proprioception. (a): Reconstruction on the standard images. When given only the images, our representation learning approach achieves results comparable to those of *Dreamer-v2* and *DRQ-v2*. Even though the images provide all information necessary to solve the tasks, our method can still exploit the proprioceptive information and improve upon the image-only baselines in both sample efficiency and final performance. (b): Contrastive variational approaches on images with natural video backgrounds. While the concatenation initially learns faster than image-only representations, only joint representations substantially improve the final performance. (c): Contrastive predictive coding approaches on images with occlusions. No approach using a single sensor is capable of solving this task. However, using both images and proprioception can give good results, in particular with *Joint(CPC+R)* and *Joint(CPC)*. Learning joint representations, allows the proprioception to shape the image features to focus on aspects that are more relevant for downstream policy learning.

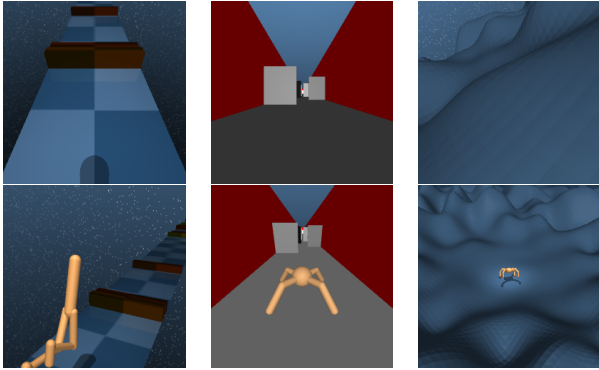


Figure 4. Example images from our Locomotion Suite. **Upper Row:** Observations provided to the agent. **Lower Row:** External images for visualization. **Left:** Similar to the cheetah in the introductory example shown in Figure 1, the walker has to walk forward while not stumbling over the hurdles placed in its way. **Center:** The ant has to move through the corridor as fast as possible, it thus needs to avoid the walls in its way. **Right:** The Quadruped has to escape a hilly landscape. This task corresponds to the standard Quadruped Escape task, where we modified the observation space by replacing the range finders with egocentric vision.

performs similarly or better than *Dreamer-v2* and *DRQ-v2*. *Img-Only(R)* also performs similarly to *DreamerPro* on the standard images, while *Img-Only(CV)* and *Img-Only(CPC)* achieve slightly worse results. However, *Img-Only(CV)* and *Img-Only(CPC)* suffer much less from adding natural videos and occlusions than *DreamerPro* and *DRQ-v2*. As expected,

none of the pure reconstruction approaches can solve the natural video and occlusion tasks, while methods that use a contrastive loss for the image perform much better. For the occluded tasks, all approaches using only images struggle to learn any reasonable behavior. While there is only a minor difference between *CV* and *CPC* methods in tasks with natural video background, *CPC* outperforms *CV* on the occlusion task. We explain this with the higher importance of learning appropriate dynamics in the occlusion tasks. It appears that *CPC*-based approaches with their explicit ahead prediction loss are better equipped to learn dynamics in this setting. Finally, combining a contrastive approach for images with reconstruction for proprioception is most of the time preferable to a purely contrastive loss.

4.2. Locomotion Suite

We propose another benchmark suite consisting of six locomotion tasks. For all tasks, we use proprioception and egocentric images. The agents need the proprioception to be aware of their own state, as they cannot observe themselves from their egocentric perspective. Moreover, the agents require egocentric images to avoid obstacles whose position and size are only available through the image. Three of the tasks are readily available with the DeepMind Control Suite (Tassa et al., 2018) and the software stack introduced in (Tassa et al., 2020). We designed three more by modifying the Cheetah Run, Walker Walk, and Walker Run tasks. Figure 4 shows some examples and Appendix A.2 provides de-

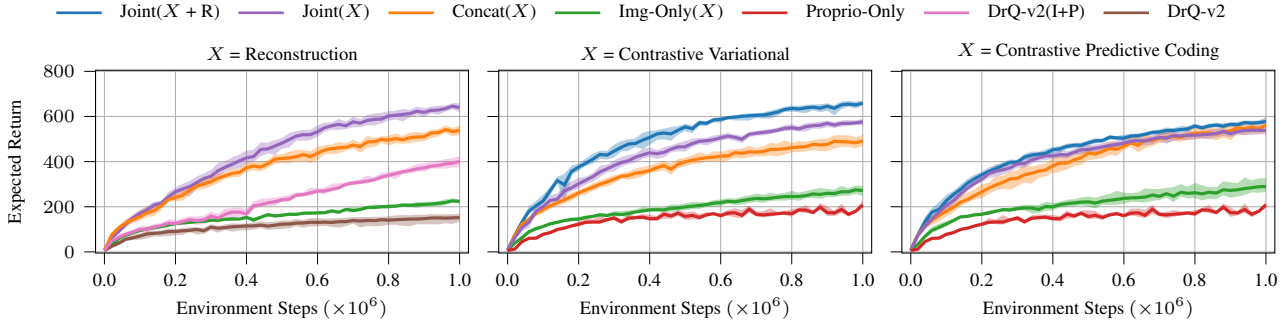


Figure 5. Aggregated results for all environments of the locomotion suite. Learning joint representations (*Joint (X)*) gives the best results with all approaches for representation learning. The joint representations clearly outperform the concatenation of image representations and proprioception, as well as *DRQ-v2*. Combining a contrastive loss for the image with reconstruction for the proprioception (*Joint (CV+R)* and *Joint (CPC+R)*) is better than using contrastive losses for both. *Joint (CV+R)* slightly outperforms the pure reconstruction approach *Joint (R)*, even though there are no distractions in the environments. Finally, the results show that using only images or only proprioception is insufficient to achieve good performance.

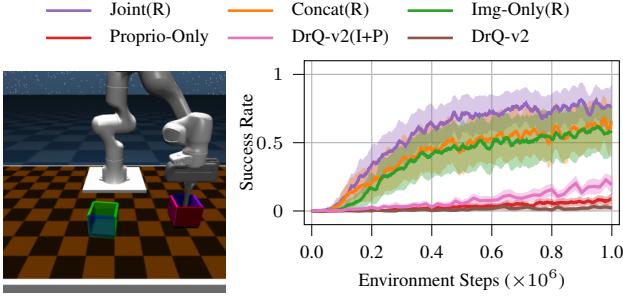


Figure 6. Example image and results for the Box Pushing task. The green box indicates the goal location, is added only for visualization, and is not visible to the agent. We evaluate 20 seeds and report the average achieved success rate. While *Concat(R)* cannot exploit the additional proprioception, using a joint representation (*Joint(R)*) improves the success rate from about 60% to over 75%.

tails about all environments. The results in Figure 5 support the previous findings that using joint representations gives the best performance of all considered methods. Again approaches that combine contrastive and reconstruction losses outperform those using only contrastive losses. In the locomotion tasks, variational methods fare better than predictive ones, as opposed to the previous experiments.

4.3. Box Pushing

For our final evaluation, we use a custom Box Pushing task. Here, a simulated seven degrees of freedom Franka Emika Panda robot has to push a box to a goal pose (position and orientation) using a rod mounted to its end-effector. We provide the positions and velocities of the seven joints as proprioception and an image to observe the box. We feed the learned representations and goal pose to the pol-

icy, which directly outputs torques for the robot’s actuators. Appendix A.3 provides further details about this setup. In this task, the challenge is to capture the complex interaction between the robot and the box, which is only observable through the image. We only use reconstruction approaches for a full-scale evaluation, as none of the contrastive methods led to reasonable behavior. The results presented in Figure 6 again highlight that using joint representations can lead to significant performance improvements.

5. Conclusion

We investigated the problem of Reinforcement Learning (RL) from multiple sensors, in particular images and proprioception. Building on *Recurrent State Space Models* (Hafner et al., 2019), we propose learning a joint representation of all available sensors instead of learning image representations in isolation. For training, we evaluated reconstruction-based and contrastive losses and showed that choosing the right loss for each type of observation yields the best results. Additionally, we considered both variational and predictive coding learning paradigms, and while neither seems preferable in general, learning joint representations is beneficial for both. Our experiments show that joint representation can significantly improve over not using proprioception for representation learning. Using proprioception can guide representation learning and allows success in settings where current image-only approaches fail.

One limitation of our current framework is its inability to use additional data for pretraining representations. For reinforcement learning and robotics, recent work (Parisi et al., 2022; Xiao et al., 2022) showed the potential of pretraining image representations on large amounts of out-of-domain data. Studying how to include such data or image representations extracted from it into our framework is a promising

avenue for future research.

References

Agarwal, R., Schwarzer, M., Castro, P. S., Courville, A. C., and Bellemare, M. Deep reinforcement learning at the edge of the statistical precipice. *Advances in neural information processing systems*, 34:29304–29320, 2021.

Ba, J. L., Kiros, J. R., and Hinton, G. E. Layer normalization. *arXiv preprint arXiv:1607.06450*, 2016.

Banijamali, E., Shu, R., Bui, H., Ghodsi, A., et al. Robust locally-linear controllable embedding. In *International Conference on Artificial Intelligence and Statistics*, pp. 1751–1759. PMLR, 2018.

Becker, P. and Neumann, G. On uncertainty in deep state space models for model-based reinforcement learning. *Transactions on Machine Learning Research*, 2022.

Brohan, A., Chebotar, Y., Finn, C., Hausman, K., Herzog, A., Ho, D., Ibarz, J., Irpan, A., Jang, E., Julian, R., et al. Do as i can, not as i say: Grounding language in robotic affordances. In *6th Annual Conference on Robot Learning*, 2022.

Cho, K., Van Merriënboer, B., Bahdanau, D., and Bengio, Y. On the properties of neural machine translation: Encoder-decoder approaches. *arXiv preprint arXiv:1409.1259*, 2014.

Deng, F., Jang, I., and Ahn, S. Dreamerpro: Reconstruction-free model-based reinforcement learning with prototypical representations. In *International Conference on Machine Learning*, pp. 4956–4975. PMLR, 2022.

Finn, C., Goodfellow, I., and Levine, S. Unsupervised learning for physical interaction through video prediction. *Advances in neural information processing systems*, 29, 2016.

Fu, Z., Kumar, A., Agarwal, A., Qi, H., Malik, J., and Pathak, D. Coupling vision and proprioception for navigation of legged robots. In *Proceedings of the IEEE/CVF Conference on Computer Vision and Pattern Recognition (CVPR)*, pp. 17273–17283, June 2022.

Ha, D. and Schmidhuber, J. World models. *arXiv preprint arXiv:1803.10122*, 2018.

Haarnoja, T., Zhou, A., Hartikainen, K., Tucker, G., Ha, S., Tan, J., Kumar, V., Zhu, H., Gupta, A., Abbeel, P., et al. Soft actor-critic algorithms and applications. *arXiv preprint arXiv:1812.05905*, 2018.

Hafner, D., Lillicrap, T., Fischer, I., Villegas, R., Ha, D., Lee, H., and Davidson, J. Learning latent dynamics for planning from pixels. In *International conference on machine learning*, pp. 2555–2565. PMLR, 2019.

Hafner, D., Lillicrap, T., Ba, J., and Norouzi, M. Dream to control: Learning behaviors by latent imagination. In *International Conference on Learning Representations*, 2020.

Hafner, D., Lillicrap, T. P., Norouzi, M., and Ba, J. Mastering atari with discrete world models. In *International Conference on Learning Representations*, 2021. URL <https://openreview.net/forum?id=0oabwyZbOu>.

Kalashnikov, D., Irpan, A., Pastor, P., Ibarz, J., Herzog, A., Jang, E., Quillen, D., Holly, E., Kalakrishnan, M., Vanhoucke, V., et al. Scalable deep reinforcement learning for vision-based robotic manipulation. In *Conference on Robot Learning*, pp. 651–673. PMLR, 2018.

Kay, W., Carreira, J., Simonyan, K., Zhang, B., Hillier, C., Vijayanarasimhan, S., Viola, F., Green, T., Back, T., Natsev, P., et al. The kinetics human action video dataset. *arXiv preprint arXiv:1705.06950*, 2017.

Kingma, D. P. and Ba, J. Adam: A method for stochastic optimization. In *ICLR*, 2015.

Kingma, D. P. and Welling, M. Auto-encoding variational bayes. *arXiv preprint arXiv:1312.6114*, 2013.

Lee, A. X., Nagabandi, A., Abbeel, P., and Levine, S. Stochastic latent actor-critic: Deep reinforcement learning with a latent variable model. *Advances in Neural Information Processing Systems*, 33:741–752, 2020.

Levine, S., Finn, C., Darrell, T., and Abbeel, P. End-to-end training of deep visuomotor policies. *The Journal of Machine Learning Research*, 17(1):1334–1373, 2016.

Ma, X., Chen, S., Hsu, D., and Lee, W. S. Contrastive variational reinforcement learning for complex observations. In *Conference on Robot Learning*, pp. 959–972. PMLR, 2020.

Mees, O., Hermann, L., and Burgard, W. What matters in language conditioned robotic imitation learning over unstructured data. *IEEE Robotics and Automation Letters*, 7(4):11205–11212, 2022.

Murphy, K. P. *Machine learning: a probabilistic perspective*. MIT press, 2012.

Nguyen, T. D., Shu, R., Pham, T., Bui, H., and Ermon, S. Temporal predictive coding for model-based planning in latent space. In *International Conference on Machine Learning*, pp. 8130–8139. PMLR, 2021.

Okada, M. and Taniguchi, T. Dreaming: Model-based reinforcement learning by latent imagination without reconstruction. In *2021 IEEE International Conference on Robotics and Automation (ICRA)*, pp. 4209–4215. IEEE, 2021.

Oord, A. v. d., Li, Y., and Vinyals, O. Representation learning with contrastive predictive coding. *arXiv preprint arXiv:1807.03748*, 2018.

Parisi, S., Rajeswaran, A., Purushwalkam, S., and Gupta, A. The unsurprising effectiveness of pre-trained vision models for control. In *International Conference on Machine Learning*, pp. 17359–17371. PMLR, 2022.

Poole, B., Ozair, S., Van Den Oord, A., Alemi, A., and Tucker, G. On variational bounds of mutual information. In *International Conference on Machine Learning*, pp. 5171–5180. PMLR, 2019.

Radford, A., Kim, J. W., Hallacy, C., Ramesh, A., Goh, G., Agarwal, S., Sastry, G., Askell, A., Mishkin, P., Clark, J., et al. Learning transferable visual models from natural language supervision. In *International Conference on Machine Learning*, pp. 8748–8763. PMLR, 2021.

Ramesh, A., Dhariwal, P., Nichol, A., Chu, C., and Chen, M. Hierarchical text-conditional image generation with clip latents. *arXiv preprint arXiv:2204.06125*, 2022.

Rezende, D. J., Mohamed, S., and Wierstra, D. Stochastic backpropagation and approximate inference in deep generative models. In *International conference on machine learning*, pp. 1278–1286. PMLR, 2014.

Shu, R., Nguyen, T., Chow, Y., Pham, T., Than, K., Ghavamzadeh, M., Ermon, S., and Bui, H. Predictive coding for locally-linear control. In *International Conference on Machine Learning*, pp. 8862–8871. PMLR, 2020.

Sohn, K., Lee, H., and Yan, X. Learning structured output representation using deep conditional generative models. *Advances in neural information processing systems*, 28: 3483–3491, 2015.

Srinivas, A., Laskin, M., and Abbeel, P. Curl: Contrastive unsupervised representations for reinforcement learning. *arXiv preprint arXiv:2004.04136*, 2020.

Srivastava, N., Talbott, W., Lopez, M. B., Zhai, S., and Susskind, J. M. Robust robotic control from pixels using contrastive recurrent state-space models. In *Deep RL Workshop NeurIPS 2021*, 2021. URL <https://openreview.net/forum?id=cRHhPrLcMRg>.

Tassa, Y., Doron, Y., Muldal, A., Erez, T., Li, Y., Casas, D. d. L., Budden, D., Abdolmaleki, A., Merel, J., Lefrancq, A., et al. Deepmind control suite. *arXiv preprint arXiv:1801.00690*, 2018.

Tassa, Y., Tunyasuvunakool, S., Muldal, A., Doron, Y., Liu, S., Bohez, S., Merel, J., Erez, T., Lillicrap, T., and Heess, N. dm_control: Software and tasks for continuous control. *Software Impacts*, 6:100022, 2020.

Wahlström, N., Schön, T. B., and Deisenroth, M. P. From pixels to torques: Policy learning with deep dynamical models. *arXiv preprint arXiv:1502.02251*, 2015.

Wang, T., Du, S., Torralba, A., Isola, P., Zhang, A., and Tian, Y. Denoised mdps: Learning world models better than the world itself. In *International Conference on Machine Learning*, pp. 22591–22612. PMLR, 2022.

Watter, M., Springenberg, J., Boedecker, J., and Riedmiller, M. Embed to control: A locally linear latent dynamics model for control from raw images. In *Advances in neural information processing systems*, pp. 2746–2754, 2015.

Wu, P., Escontrela, A., Hafner, D., Abbeel, P., and Goldberg, K. Daydreamer: World models for physical robot learning. In *6th Annual Conference on Robot Learning*, 2022.

Xiao, T., Radosavovic, I., Darrell, T., and Malik, J. Masked visual pre-training for motor control. *arXiv preprint arXiv:2203.06173*, 2022.

Yarats, D., Fergus, R., Lazaric, A., and Pinto, L. Reinforcement learning with prototypical representations. In *International Conference on Machine Learning*, pp. 11920–11931. PMLR, 2021a.

Yarats, D., Zhang, A., Kostrikov, I., Amos, B., Pineau, J., and Fergus, R. Improving sample efficiency in model-free reinforcement learning from images. In *Proceedings of the AAAI Conference on Artificial Intelligence*, volume 35, pp. 10674–10681, 2021b.

Yarats, D., Fergus, R., Lazaric, A., and Pinto, L. Mastering visual continuous control: Improved data-augmented reinforcement learning. In *International Conference on Learning Representations*, 2022. URL https://openreview.net/forum?id=_SJ-_yyes8.

You, B., Arenz, O., Chen, Y., and Peters, J. Integrating contrastive learning with dynamic models for reinforcement learning from images. *Neurocomputing*, 476:102–114, 2022.

Zhang, A., McAllister, R. T., Calandra, R., Gal, Y., and Levine, S. Learning invariant representations for reinforcement learning without reconstruction. In *International Conference on Learning Representations*, 2020.

Environment	Proprioceptive	Non-Proprioceptive
Ball In Cup	cup position and velocity	ball position and velocity
Cartpole	cart position and velocity	pole angle and velocity
Cheetah	joint positions and velocities	global pose and velocity
Reacher	reacher position and velocity	distance to target
Quadruped	joint positions and velocities	global pose + velocity, forces
Walker	orientations and velocities of links	global pose and velocity, height above ground

Table 1. Splits of the entire system state into proprioceptive and non-proprioceptive parts for the DeepMind Control Suite environments.

Environment	Proprioceptive	Non-Proprioceptive
Ant	joint position and velocity global velocities	wall positions global position
Hurdle Cheetah	joint positions and velocities global velocity	hurdle positions and heights global position
Hurdle Walker	orientations and velocities of links	hurdle positions and height global position and velocity
Quadruped (Escape)	joint positions and velocities, torso orientation and velocity, imu, forces, and torques at joints	Information about terrain

Table 2. Splits of the entire system state into proprioceptive and non-proprioceptive parts for the Locomotion Suite. Some of the agents (Cheetah, Walker, Quadruped) require more proprioceptive information for the locomotion tasks with an egocentric vision than for the standard tasks with images from an external perspective.

A. Environments

A.1. DeepMind Control Suite Tasks

Table 1 states how we split the states of the original DeepMind Control Suite (Tassa et al., 2018) tasks into proprioceptive and non-proprioceptive parts. Table 3 shows the action repeats for the individual environments.

Natural Background. Following (Nguyen et al., 2021; Zhang et al., 2020; Deng et al., 2022) we used the videos from the driving car class of the Kinetics400 dataset (Kay et al., 2017). We used all available videos in the dataset and adhered to the train-validation split, using the first for representation and policy learning and the latter during evaluation.

Occlusions. Following (Becker & Neumann, 2022), we rendered slow-moving disks over the original observations to occlude parts of the observation. The speed of the disks makes memory necessary, as they can occlude relevant aspects for multiple consecutive timesteps.

A.2. Locomotion Suite

The 6 tasks in the locomotion suite are Ant Empty, Ant Walls, Hurdle Cheetah Run, Hurdle Walker Walk, Hurdle Walker Run, and Quadruped Escape. Table 2 shows the splits into proprioceptive and non-proprioceptive parts. Figure 7 displays all environments in the suite.

Ant. The Ant tasks build on the locomotion functionality introduced into the DeepMind Control suite by (Tassa et al., 2020). For Ant Empty, we only use an empty corridor, which makes this the easiest task in our locomotion suite. For Ant Walls, we randomly generate walls inside the corridor, and the agent has to avoid those in order to achieve its goal, i.e., running through the corridor as fast as possible.

Hurdle Cheetah & Walker. We modified the standard Cheetah Run, Walker Walk, and Walker Run tasks by introducing “hurdles” over which the agent has to step in order to move forward. The hurdles’ positions, heights, and colors are reset

Environment	Action Repeat	Environment	Action Repeat
Deep Mind Control Suite Tasks		Locomotion Suite	
Ball In Cup Catch	4	Ant Empty & Walls	2
Cartpole Swingup	8	Cheetah Run	2
Cheetah Run	4	Quadruped Escpae	2
Reacher Easy	4	Walker Walk & Run	2
Quadruped Walk	2		
Walker Walk & Run	2		

Table 3. Action Repeats for standard DeepMind Control Suite (Tassa et al., 2018) and the locomotion suite. We changed the action repeat for the cheetah between the standard and locomotion tasks as we find that avoiding the obstacles requires more fine-grained control.

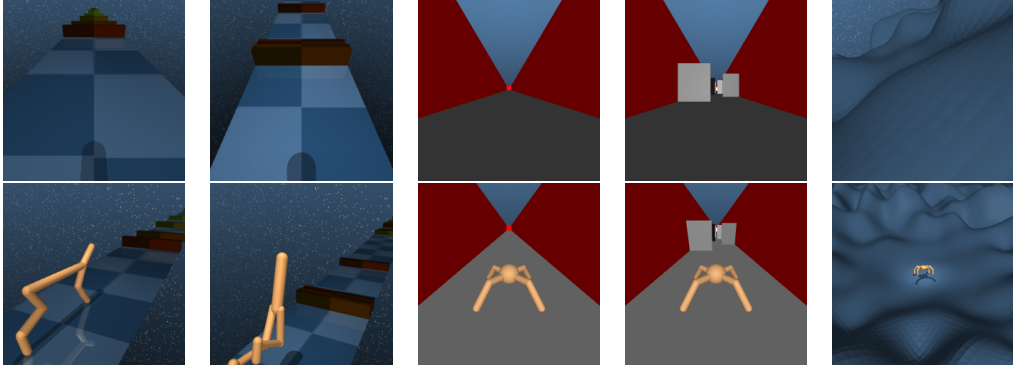


Figure 7. The environments in the Locomotion Suite are (from left to right) Hurdle Cheetah Run, Hurdle Walker Walk / Run, Ant Empty, Ant Walls, and Quadruped Escape. **Upper Row:** Egocentric vision provided to the agent. **Lower Row:** External image for visualization.

randomly for each episode, and the agent has to perceive them using egocentric vision. For this vision, we added a camera in the head of the Cheetah and Walker.

Quadruped Escape. The Quadruped Escape task is readily available in the DeepMind Control Suite. For the egocentric vision, we removed the range-finding sensors from the original observation and added an egocentric camera.

A.3. Box Pushing.

For the Box Pushing tasks we only actively controlled the first 6 degrees of freedom, as the final joint only rotates the rod, which has no effect. The reward consists of three terms, the Euclidean distance of the rod to the center of the box, the Euclidean distance between the box and the target position, and the angular distance between box orientation and target orientation divided by π . We used the `tolerance` function of the Deep Mind Control Suite (Tassa et al., 2018) to map the values into the interval $[0, 1]$ and took a weighted sum. The distance of the rod to the box has a weight of 0.2, while the other two have 0.4. We consider a rollout as successful if the box is closer to the target than 5cm in position and 0.5 Rad in orientation.

B. Hyperparameters and Architecture

We used the same hyperparameters in all experiments with the exception of the Box Pushing. For tasks, we increased the number of free nats for the state space representation (see below) from 1 to 3.

B.1. Recurrent State Space Model

The base-*RSSM* model without parts specific to one of the objectives consists of:

- **Encoders:** $\psi_{\text{obs}}^{(k)}(\mathbf{o}_t)$, where ψ_{obs} is the convolutional architecture proposed by (Ha & Schmidhuber, 2018) and used by

(Hafner et al., 2019; 2020) for image observations and a 3×400 Units fully connected NN with ELU activation for proprioceptive observations (, i.e., vectors).

- **Deterministic Path:** $\mathbf{h}_t = g(\mathbf{z}_{t-1}, \mathbf{a}_{t-1}, \mathbf{h}_{t-1}) = \text{GRU}(\psi_{\text{det}}(\mathbf{z}_{t-1}, \mathbf{a}_{t-1}), \mathbf{h}_{t-1})$, where ψ_{det} is 2×400 units fully connected NN with ELU activation and the GRU has a memory size of 200.
- **Dynamics Model:** $p(\mathbf{z}_{t+1}|\mathbf{z}_t, \mathbf{a}_t) = \psi_{\text{dyn}}(\mathbf{h}_t)$, where ψ_{dyn} is a 2×400 units fully connected NN with ELU activation. The network learns the mean and standard deviation of the distribution.
- **Variational Distribution** $q(\mathbf{z}_t|\mathbf{z}_{t-1}, \mathbf{a}_{t-1}, \mathbf{o}_t) = \psi_{\text{var}}\left(\mathbf{h}_t, \text{Concat}\left(\{\psi_{\text{obs}}^{(k)}(\mathbf{o}_t^{(k)})\}_{k=1:K}\right)\right)$, where ψ_{var} is a 2×400 units fully connected NN with ELU activation. The network learns the mean and standard deviation of the distribution.
- **Reward Predictor** $p(r_t|\mathbf{z}_t)$: 2×128 units fully connected NN with ELU activation. The network only learns the mean of the distribution. The standard deviation is fixed at 1.

B.2. Objectives

Image Inputs and Preprocessing. For the reconstruction objective, we used images of size 64×64 pixels as input to the model. For the contrastive objectives, the images are of size 76×76 pixel image and we used 64×64 pixel random crops. Cropping is temporally consistent, i.e., we used the same crop for all time steps in a sub-sequence. For evaluation, we took the crop from the center.

Reconstruction Objectives. Whenever we reconstructed images we used the up-convolutional architecture proposed by (Ha & Schmidhuber, 2018) and used by (Hafner et al., 2019; 2020). For low-dimensional observations, we used 3×400 units fully connected NN with ELU activation. In all cases, only the mean is learned and the standard deviation is fixed at 1.

For the KL term in Equation 1, we combine the KL-Balancing technique introduced in (Hafner et al., 2021) with the *free-nats regularization* used in (Hafner et al., 2019; 2020). Following (Hafner et al., 2021) we use a balancing factor of 0.8. We give the algorithm 1 free nat for the DeepMind Control Suite and the Locomotion Suite tasks and 3 for the Box Pushing.

Contrastive Variational Objective. The score function for the contrastive variational objective is given as

$$f_v^{(k)}(\mathbf{o}_t^{(k)}, \mathbf{z}_t) = \exp\left(\frac{1}{\lambda} \rho_o\left(\psi_{\text{obs}}^{(k)}(\mathbf{o}_t)\right)^T \rho_z(\mathbf{z}_t)\right),$$

where $\psi_{\text{obs}}^{(k)}$ is the RSSM’s encoder and λ is a learnable inverse temperature parameter. ρ_o and ρ_z are projections that project the embedded observation and latent state to the same dimension, i.e., 50. ρ_o is only a single linear layer while ρ_z is a 2×256 fully connected NN with ELU activation. Both use LayerNorm (Ba et al., 2016) at the output.

Contrastive Predictive Objective. The score function of the contrastive predictive objective looks similar to the one of the contrastive variational objective. The only difference is that the latent state is forwarded in time using the RSSMs transition model to account for the predictive nature of the objective,

$$f_p^{(k)}(\mathbf{o}_{t+1}^{(k)}, \mathbf{z}_t) = \exp\left(\frac{1}{\lambda} \rho_o\left(\psi_{\text{obs}}^{(k)}(\mathbf{o}_{t+1})\right)^T \rho_z(\phi_{\text{dyn}}(g(\mathbf{z}_t, \cdot)))\right).$$

We use the same projections as in the contrastive variational case.

Following (Srivastava et al., 2021) we scale the KL term using a factor of $\beta = 0.001$ and parameterize the inverse dynamics predictor as a 2×128 unit fully connected NN with ELU activations.

Optimizer. We used Adam (Kingma & Ba, 2015) with $\alpha = 3 \times 10^{-4}$, $\beta_1 = 0.99$, $\beta_2 = 0.9$ and $\varepsilon = 10^{-8}$ for all losses.

B.3. Soft Actor Critic

Table 4 lists our SAC-Hyperparameters.

B.4. Data Collection and Learning

We collected 5 initial sequences at random. During training, we update the RSSM, critic, and actor in an alternating fashion for d steps before collecting a new sequence. Here, d is set to be half of the environment steps collected per sequence (after accounting for potential action repeats).

Hyperparameter	Value
Actor Hidden Layers	$3 \times 1,024$ Units
Actor Activation	ELU
Critic Hidden Layers	$3 \times 1,024$ Units
Critic Activation	ELU
Discount	0.99
Actor Learning Rate	0.001
Actor Gradient Clip Norm	10
Critic Learning Rate	0.001
Critic Gradient Clip Norm	100
Target Critic Decay	0.995
Target Critic Update Interval	1
α learning rate	0.001
initial α	0.1
target entropy	- action dim

Table 4. Hyperparameters used for policy learning with the Soft Actor-Critic.

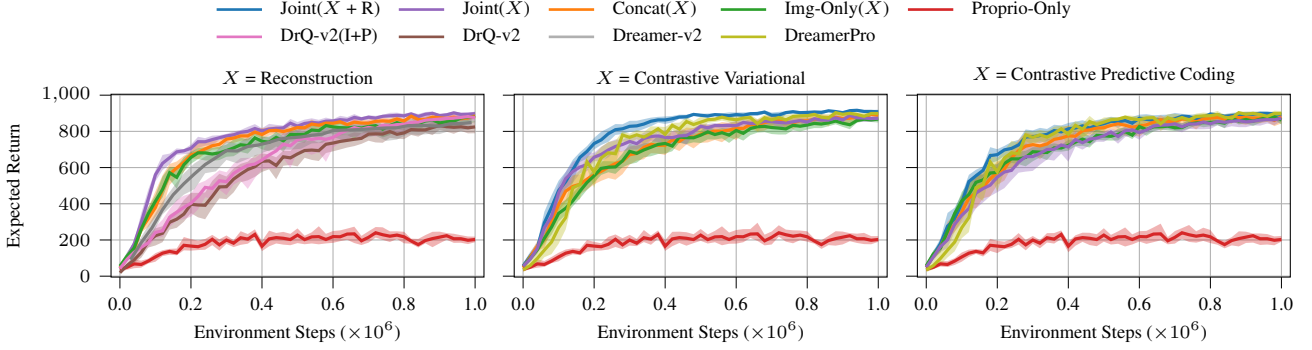


Figure 8. Aggregated Results for the DMC Suite task with standard images. (*Img-Only(R)*) achieves similar performance to *Dreamer-v2*, *DrQ-v2*, and *DreamerPro*, showing that our representation learning approach also works without multiple sensors. However, using both images and proprioception is still advantageous in these tasks, and using joint representations leads to larger performance gains.

C. Additional Results

Here we list the aggregated results for all methods on the DeepMind Control (DMC) Suite with standard images (Figure 8), natural video background (Figure 9), and occlusions (Figure 10)

C.1. Results for Individual Environments.

The following figures provide the per environment results for the DMC Suite with standard images (Figure 11), with natural video background (Figure 12), with occlusion (Figure 13), and for the Locomotion Suite (Figure 14). We again report interquartile means and 95% bootstrapped confidence intervals (Agarwal et al., 2021).

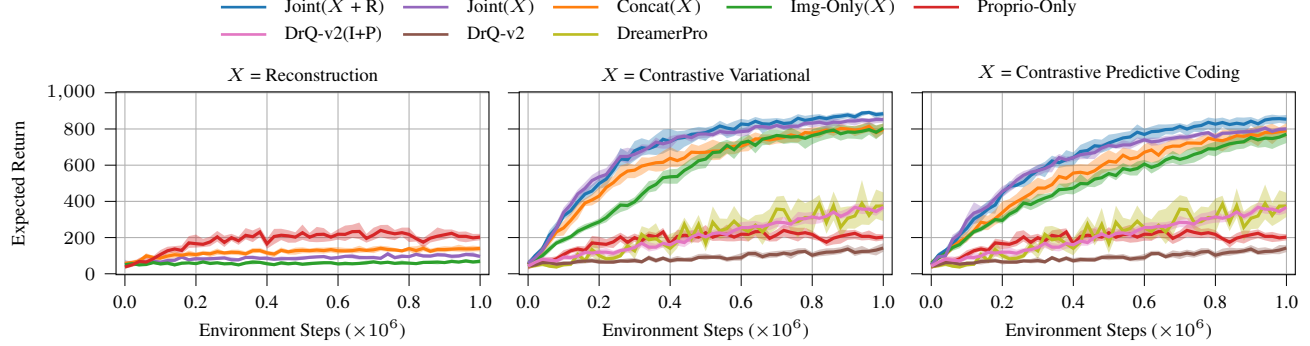


Figure 9. Aggregated Results for the DMC Suite task with natural video background. As expected, all purely reconstruction-based approaches fail at the task, while those using a contrastive loss for the images achieve better results. The results are consistent between contrastive variational and predictive coding approaches. For both *ConcatX* only improves the sample efficiency while joint representation learning can also increase the final performance. Using a contrastive image loss in combination with reconstruction for proprioception gives the best results.

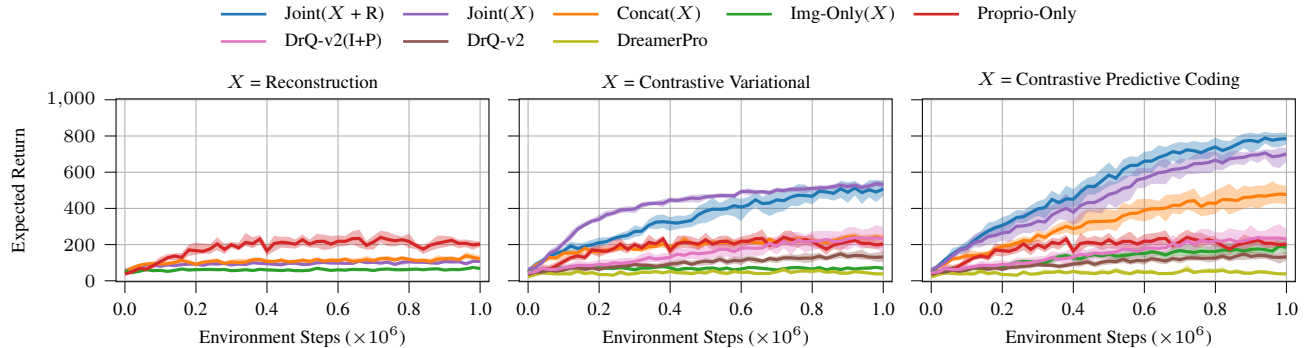


Figure 10. Aggregated Results for the DMC Suite task with occlusion. In this task now method that uses only images or reconstructs images performs better than solely using proprioception. However, combining both modalities and using contrastive methods for the images leads to vast performance improvements. While at least for contrastive predictive coding, these improvements are already significant for the concatenation approach, joint representation learning gives even more performance. In this task, the contrastive predictive coding methods outperform contrastive variational ones, arguably because their explicit ahead prediction allows them to learn better dynamics.

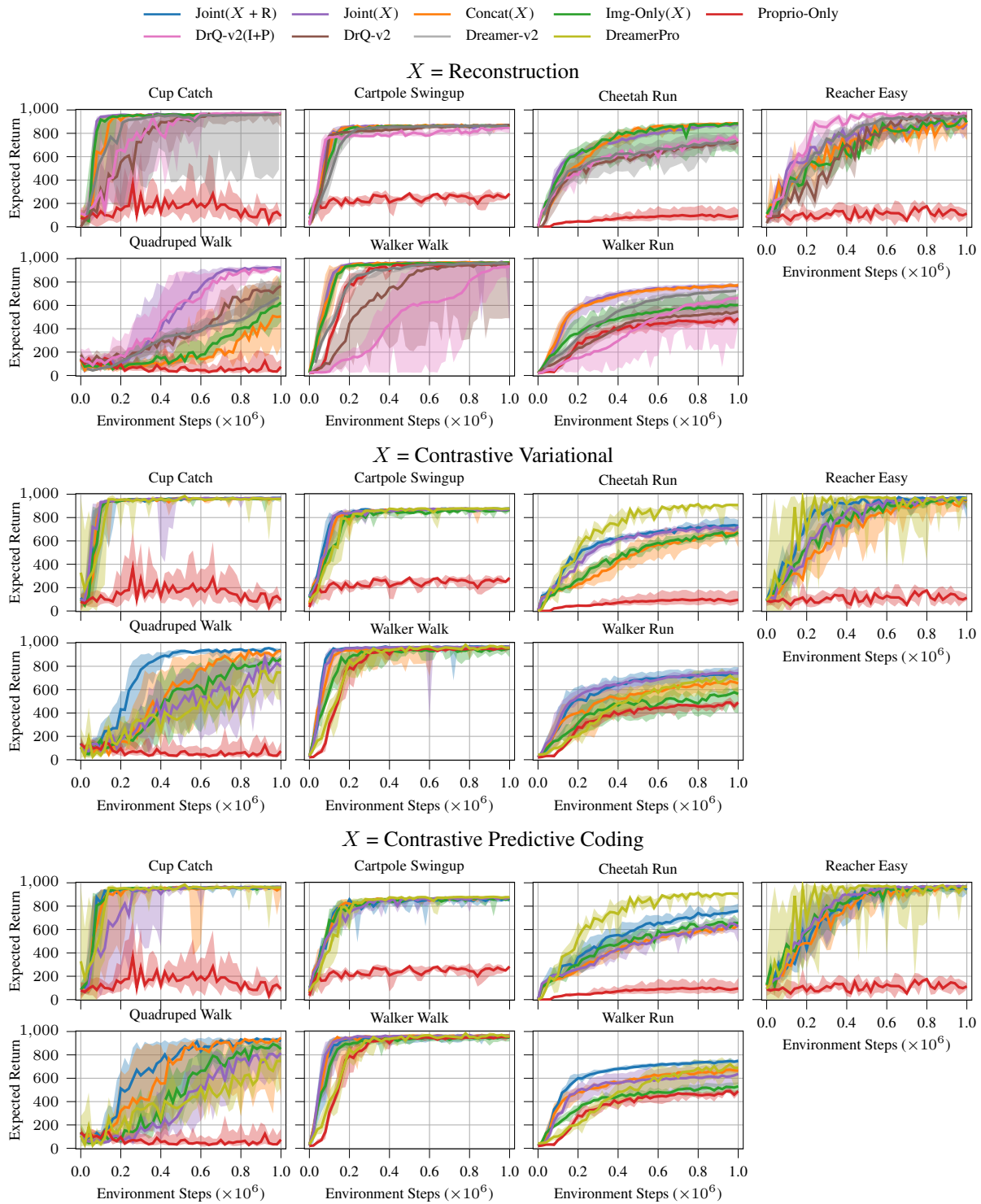


Figure 11. Per environment results for the DMC Suite with standard images.

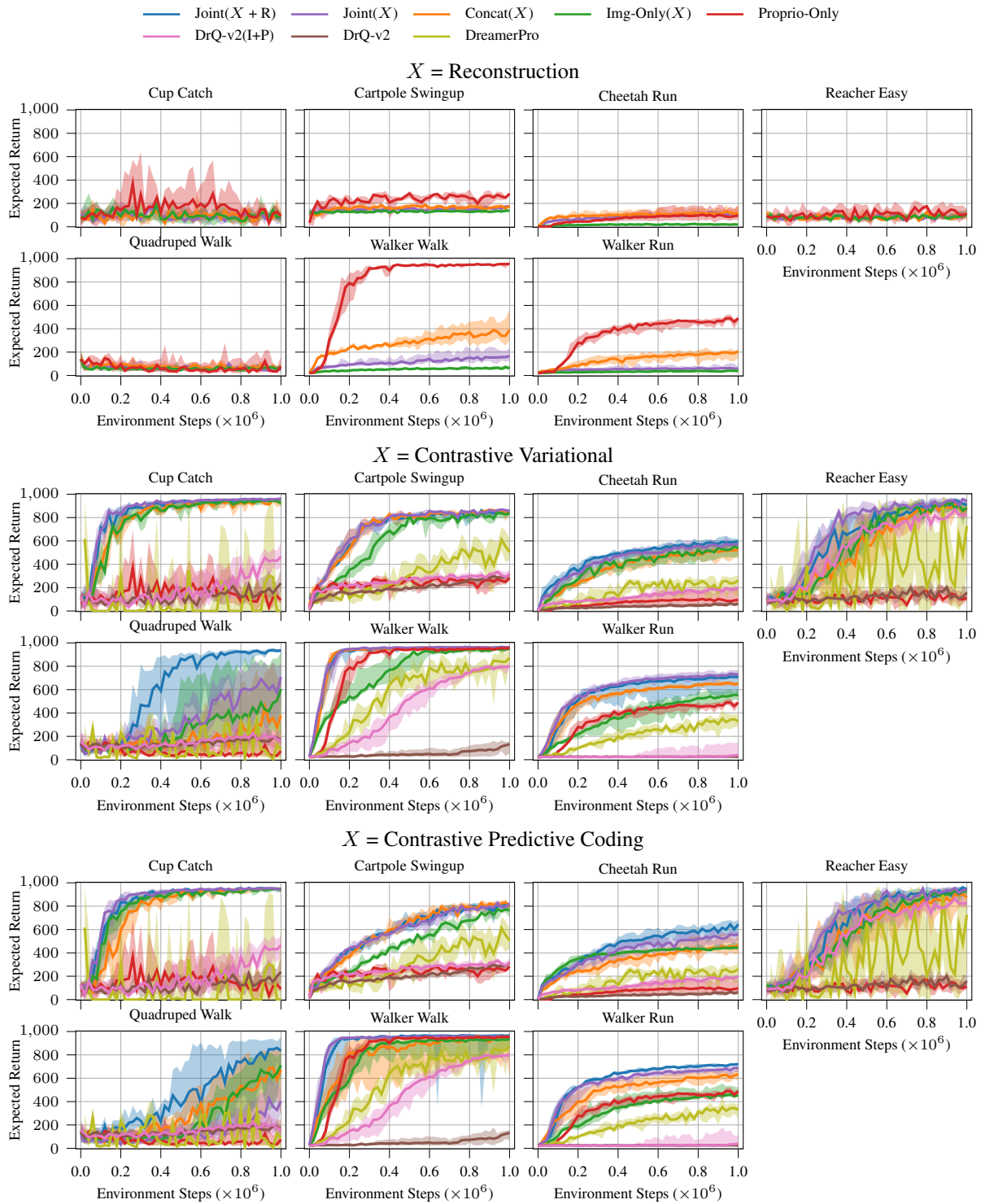


Figure 12. Per environment results for the DMC Suite with natural video background.

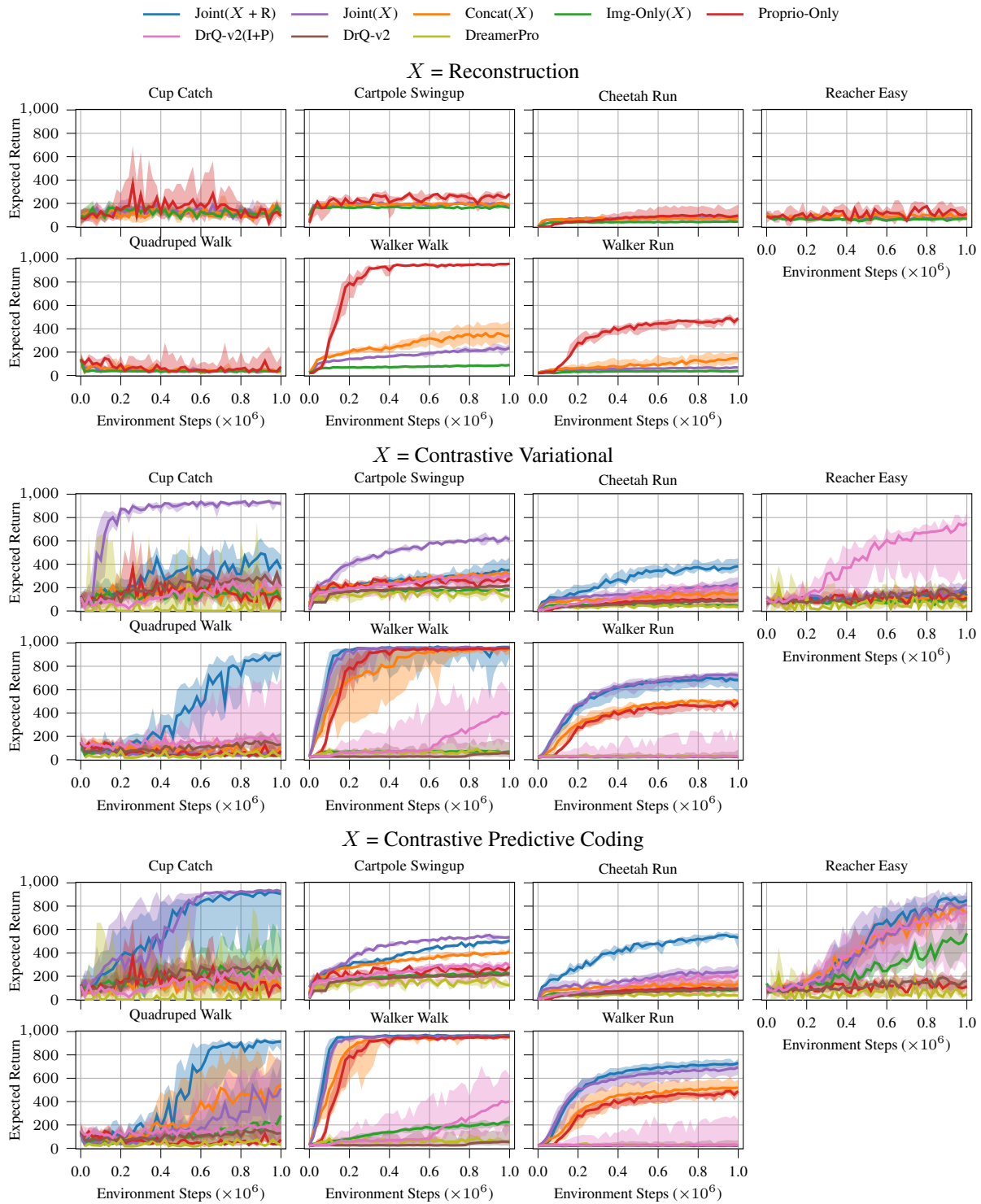


Figure 13. Per environment results for the DMC Suite with occluded images.

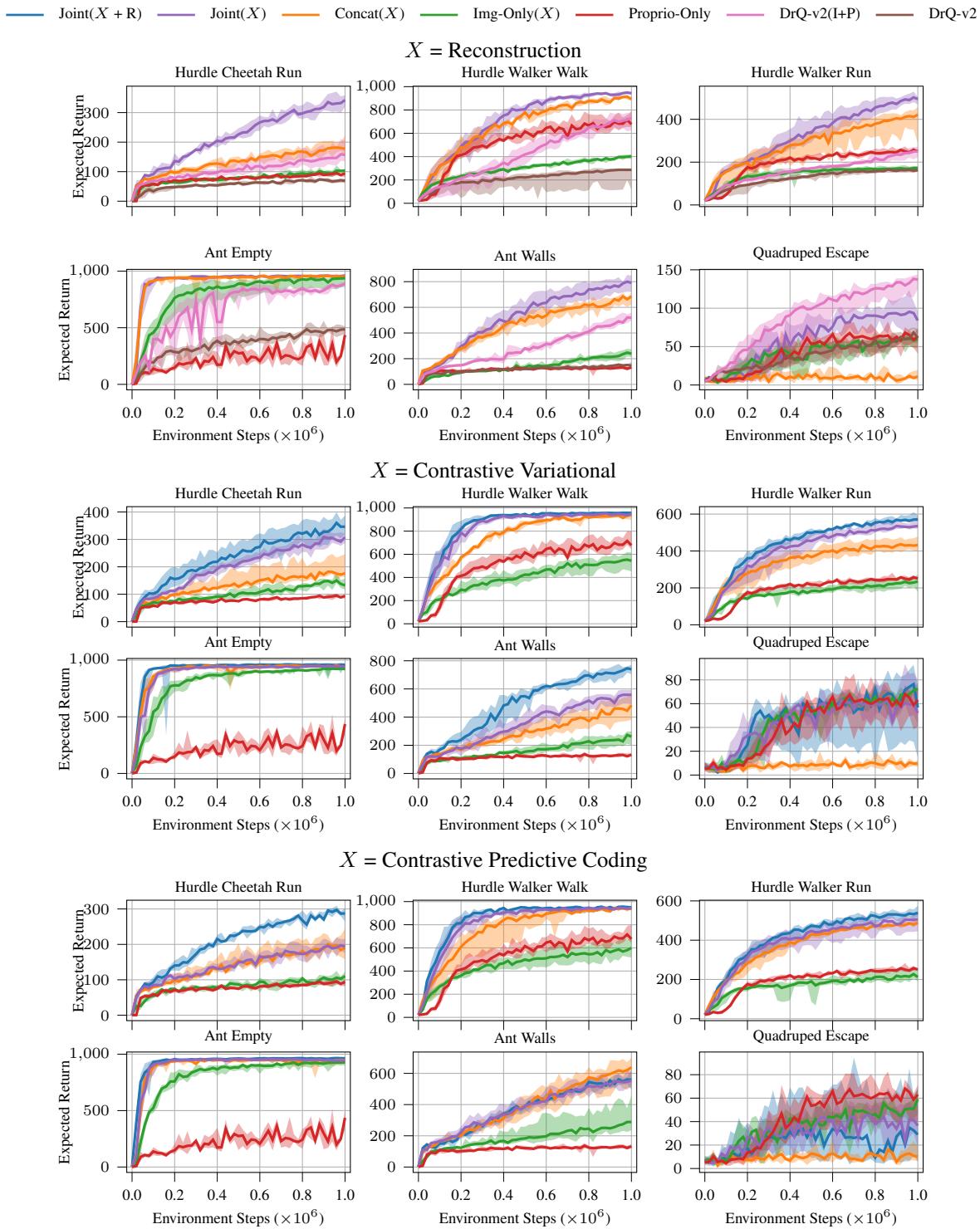


Figure 14. Per environment results for the Locomotion Suite.